DISTAL FLOWS ASSOCIATED WITH SOME OF THE BEST-PRESERVED CRATERS ON MARS: IMPLICATIONS FOR EXTENSIVE IMPACT-RELATED LANDSCAPE MODIFICATION (AN UPDATE).

J. M. Burley[1,2], L. L. Tornabene[1,2], G. R. Osinski[1,2], J. A. Grant[3], M. R. El-Maarry[4], [1]Department of Earth Sciences, Western University, London, ON, Canada (jburley6@uwo.ca), [2]Institute for Earth & Space Exploration, Western University, London, ON, Canada, [3]Center for Earth & Planetary Studies, National Air & Space Museum, Smithsonian Institution, 6th at Independence SW, Washington, DC, 20560 (grantj@si.edu), [4]Space & Planetary Science Center & Department of Earth Sciences, Khalifa University, Abu Dhabi, UAE (mohamed.elmaarry@ku.ac.ae)

Introduction: We explore well-preserved craters on Mars where extensive surface flow morphologies (here defined as Distal Flow Deposits or DFDs) are observed predominantly beyond the range of proximal ejecta (cf. [1, 2]). DFDs were first identified on Mars beyond the rugged layered ejecta blanket in 2008 [3] at Hale crater (D ~125x150 km). Since then, a total of four craters on Mars have had such flows characterized, namely Hale [4, 5, 6], Noord (D ~7 km) [2], Resen (D ~7.5 km) [2], and an unnamed crater in Noachis Terra (D ~9 km) [1]. Despite this small sample, a growing set of candidate DFD-bearing craters [1, 2] has been identified. In addition, strong evidence for an extensive region of continuous modification around craters on Mars [7, 8, 9] implies currently understood impact-induced landscape modification requires further investigation. Here we expand DFD characterization to four new candidate craters with an aim to better constrain these potentially globally-applicable emplacement mechanisms.

Methods: Craters were selected from a list of HiRISE verified martian DFD candidates identified via global survey [1, 10]. Focusing on 6 craters (two previously reported and four new, see Figure 1), this work utilizes a multitude of sensors including HiRISE, CaSSIS, CTX, and THEMIS (TIR) for visual interpretation, mapping, and morphometric analysis of distal flow morphologies and their relationship to proposed source craters. Using stereo derived DTMs, we provide morphometric constraints on whether a fluidized or gravity driven dry emplacement mechanism best explains each flow feature. Elevation models used for such morphometric analysis are derived using the Ames Stereo Pipeline [11].

In addition to previously described geomorphic interpretation strategies, terrain age data for DFD craters and surrounding target materials are also investigated here using mapped DFD constraints and available crater chronologies for a single candidate [12] (Figure 1, yellow table, 9 km D).

Observations: Distal flow accumulations at all the studied locations appear to express two distinct morphologies similar to those previously described in Noachis Terra [1] (Figure 1). Type 1 exhibits accumulation of material at the base of topographic positive relief obstacles, preferentially on the side of the obstacle facing the source crater (see Figure 1, Type 1 Flow). Deposit volumes are observed to visually reduce when moving from the slope facies of obstacles that directly face the well-preserved crater (i.e., normal to the crater) to a point where the deposits are notably absent on the opposing side of said obstacles (see Occluded Terrain in Figure 1).

Type 2 characterizes flows that are generally observed where steep pre-existing slopes associated with topography create valleys (see Figure 1, Type 2 Flows). On terraces & other low-slope surfaces above such morphologies, flow materials are observed to coalesce before channelizing into Type 2.

Slope modelling for flows shown in Figure 1 finds DFDs channelize on terrains when traversing slopes <20º, with flow morphologies becoming muted beyond recognition on terrains with slope values <5º. Maximum surface slope values for individual Type 1 and Type 2 DFDs vary somewhat depending on topographic variabilities of the underlying terrain, though are both observed almost exclusively <20º. In terms of DFD runout distances for candidate craters assessed to date, discernable flows of both types are observed beyond the continuous ejecta blanket with the majority of identifiable DFDs observed at distances ≤7 R from impact center. Though less abundant at distance >7 R, flows sometimes extend further, with the most distal example of DFDs recorded for the candidates in this report being a type 1 flow at a distance of ≈ 12 R – Similar to that noted for lunar flows found on crater-facing slopes [13].

Though age dating of individual flows is not feasible given the scale constraints of crater counting, crater chronologies for the unnamed crater in Noachis Terra (Figure 1, table , yellow, 9 km Diameter) suggest the supposed source impact occurred <14 Ma, though no more recently than 6 Ma [12].

Discussion and Future Works: Where data is available at appropriate resolutions, DFDs continue to express slope values exclusively indicative of viscous or fluidized material emplacement. DFDs and the two ways they are predominantly observed to interact with target terrains can be explained via the mechanism of radially expansive ground hugging flow(s) outward from the impact crater. Deposition of hot and/or fluid impact ejecta on ballistic trajectories is also possible, though this mechanism would rely on oblique trajectories given occluded terrain and their implications for topographic shadowing effects.

Crater D. (km)*	Center Lat. N, Long. E	Target Description
19	4.95°, 21.78°	Arabia Terra (unnamed)
12	**4.45°, 106.8°**	**Amenthes Planum (unnamed)**
11.5	-35.2°, 201.6°	Sirenum Terra (unnamed)
3	0.83°, 319.77°	Xanthe Terra (unnamed)
9	-29.41°, 351.32°	Noachis Terra (unnamed)
7	-19.27°, 348.73°	Noachis Terra (Noord)

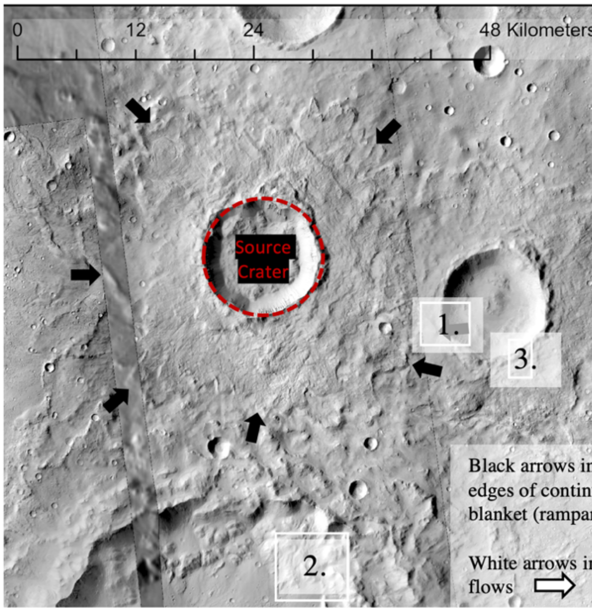

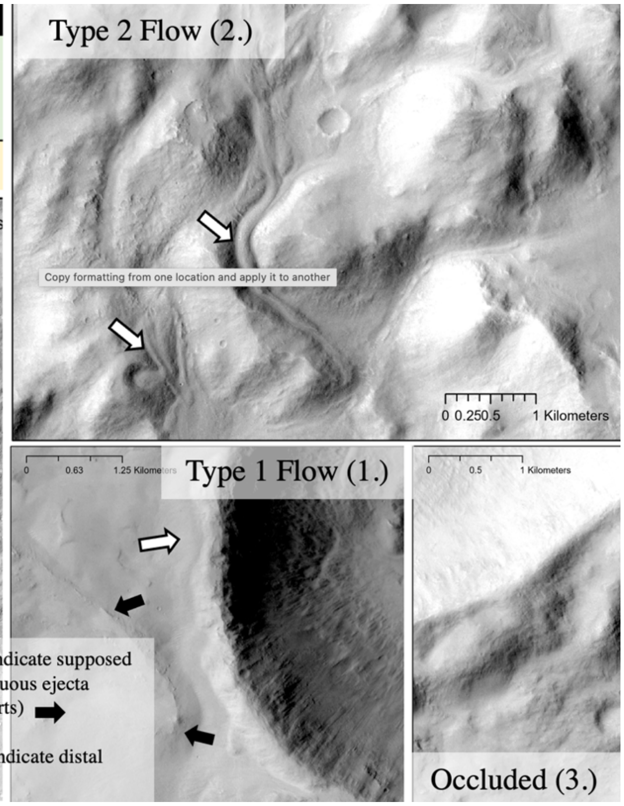

Figure 1. Context map for a candidate/source crater is shown (left) with associated DFDs and target terrains described at higher magnifications (right). Candidate craters reviewed in this report are identified in a colourized table. Novel candidates are symbolized in the table in green, those previously reported are in yellow. Crater exampled in the CTX images has boldened text in table of candidates (12 km D, 4.45ºN x 206.8ºE, Amenthes).

Though slope characteristics and directional bias of emplaced DFDs are indicative of fluidized ground-hugging flow, more information is needed to constrain whether flows were kinematically/atmospherically dry fluidized or at least partially viscous upon emplacement. Potential factors associated with the fluidization or viscous mobilization of target materials include impact generated winds (surface abrading/entraining) [7], collapsing impact plume materials [14], pyroclastic/lahar-like ejecta material interactions [15, 13], and thermal radiation [16].

Though the current sample of age dated DFD candidate craters is too small for global interpretations, initial findings of candidate crater ages being on the order of 10 Ma supports arguments that DFD expression is at least partially if not predominantly a function of crater preservation. Given martian planetary obliquity patterns over this time period [17] and the latitudinal locations of these craters, these impacts may have occurred into more volatile-rich target substrates than are present today. Whether volatile-rich substrates are necessary for DFD morphologies to develop remains unconstrained and will continue to be explored.

Future developments of this work include the continued characterization of newly identified flow candidates where DFDs might be better captured to expose their mechanisms of emplacement, hazard, or potential resources.

References: [1] Burley et al. (2022) *LPSC 53.,* #1619. [2] Tornabene et al. (2019) *Mars 9.,* #2089. [3] Tornabene el al. (2008) *LPSC 35.,* #2180. [4] Jones et al. (2011) *Icarus*, 211, 259–272. [5] El-Maarry et al (2013) *Icarus,* 226, 905–922. [6] Grant and Wilson (2018) *Meteoritics*, 53, 839–856. [7] Ghent et al (2010*) Icarus, 209*, 818–835. [8] Barlow et al (2014) *Icarus*, 239, 186-200. [9] Boyce et al (2015) *Icarus,* 245, 263-272. [10] Tornabene et al. 2012. *Icarus, 220*. [11] Beyer et al. (2018) *Earth and Space Sci. 5,* 537–548. [12] Lagain et al. (2021) *Nature Comms,* 12, 6352. [13] Bray et al. (2018) *Icarus*, 301, 26–36. [14] Trolese et al. (2019) *Nature Comms*, 10, 2476. [15] Sigursson (2015). *Ency. of Volc. Ch.35-37*. [16] Svetsov & Shuvalov (2019) *Meteoritics, 54,* 126–141. [17] Laskar et al. (2004) *Icarus*, 170, 343-364.

Acknowledgements: We thank the spacecraft & instrument engineering teams for the successful completion of the instruments. The lead author acknowledges support from Tornabene's funding from the CSA's Planetary and Astronomy Missions Co-Investigator programme (22EXPCOI3) and the Canadian NSERC Discovery Grant programme (06418-2020 RGPIN).